

RESEARCH ARTICLE | JANUARY 04 2024

# Laser beam properties and microfluidic confinement control thermocavitation

Jelle J. Schoppink   ; Jose A. Alvarez-Chavez  ; David Fernandez Rivas 



*Appl. Phys. Lett.* 124, 014102 (2024)

<https://doi.org/10.1063/5.0186998>



CrossMark



**APL Quantum**  
Bridging fundamental quantum research with technological applications

**Now Open for Submissions**  
No Article Processing Charges (APCs) through 2024

**Submit Today**



# Laser beam properties and microfluidic confinement control thermocavitation

Cite as: Appl. Phys. Lett. **124**, 014102 (2024); doi: 10.1063/5.0186998

Submitted: 10 November 2023 · Accepted: 16 December 2023 ·

Published Online: 4 January 2024






View Online



Export Citation



CrossMark

Jelle J. Schoppink,<sup>1,a)</sup>  Jose A. Alvarez-Chavez,<sup>2</sup>  and David Fernandez Rivas<sup>1</sup> 

## AFFILIATIONS

<sup>1</sup>Mesoscale Chemical Systems group, MESA+ Institute and Faculty of Science and Technology, University of Twente, P.O. Box 217, 7500 AE Enschede, The Netherlands

<sup>2</sup>Optical Sciences group, MESA+ Institute and Faculty of Science and Technology, University of Twente, P.O. Box 217, 7500 AE Enschede, The Netherlands

<sup>a)</sup>Author to whom correspondence should be addressed: [jj.schoppink@utwente.nl](mailto:jj.schoppink@utwente.nl)

## ABSTRACT

Thermocavitation, the creation of a vapor bubble by heating a liquid with a continuous-wave laser, has been studied for a wide range of applications. Examples include the development of an actuator for needle-free jet injectors, as the pumping mechanism in microfluidic channels and nanoparticle synthesis. Optimal use in these applications requires control over the bubble dynamics through the laser power and beam radius. However, the influence of the laser beam radius on the bubble characteristics is not fully understood. Here, we present a way to control the beam radius from an optical fiber by changing the distance from the glass–liquid interface. We show that the increase in the beam size results in a longer nucleation time. Numerical simulations of the experiment show that the maximum temperature at nucleation is  $237 \pm 5^\circ\text{C}$  and independent of laser parameters. Delayed nucleation for larger beam sizes results in more absorbed energy by the liquid at the nucleation instant. Consequently, a larger beam size results in a faster growing bubble, producing the same effect as reducing the laser power. We conclude that the bubble energy only depends on the amount of absorbed optical energy and it is independent of the beam radius and laser power for any amount of absorbed energy. This effect contrasts with pulsed lasers, where an increase in the beam radius results in a reduction of bubble energy. Our results are of relevance for the use of continuous-wave laser-actuated cavitation in needle-free jet injectors as well as other applications of thermocavitation in microfluidic confinement.

© 2024 Author(s). All article content, except where otherwise noted, is licensed under a Creative Commons Attribution (CC BY) license (<http://creativecommons.org/licenses/by/4.0/>). <https://doi.org/10.1063/5.0186998>

The creation of a vapor bubble by heating the liquid with a continuous-wave (CW) laser was first reported in 1987 by Rastopov and Sukhodol'skii, who called it thermocavitation.<sup>1</sup> Since then, thermocavitation has been studied for numerous applications, including removal of pathological tissues,<sup>2</sup> nanoparticle synthesis,<sup>3</sup> laser-induced crystallization,<sup>4</sup> as pumping mechanism in a microchannel,<sup>5</sup> creation of short laser pulses,<sup>6</sup> generation of ultrasound acoustics,<sup>7–9</sup> and trapping or manipulation of bubbles.<sup>10,11</sup> Over the last decade, thermocavitation also has been investigated for its potential to create microfluidic jets for needle-free jet injection.<sup>12–15</sup> Although laser-actuated jet injection was initially studied using pulsed lasers,<sup>16–20</sup> recently we found that continuous-wave lasers generate similar bubble dynamics.<sup>21</sup> For all of these applications of thermocavitation, understanding and control of the bubble formation is vital.

However, a thorough understanding of the thermocavitation process is still lacking. Due to the low laser power ( $P \sim 1\text{ W}$ ), the bubble does not form instantaneously upon laser irradiation, but after a short

incubation time ( $t_n \sim \text{ms}$ ). Therefore, the delivered optical energy  $E_d$  is not controlled directly, but depends on the bubble nucleation instant ( $E_d = P \times t_n$ ).<sup>21</sup> Delaying this nucleation time  $t_n$  therefore, increases the amount of energy, resulting in a larger bubble.<sup>22,23</sup> This can be achieved by reducing the laser power, where heat dissipation further increases the nucleation time and therefore increases the energy,<sup>22,24</sup> or absorption coefficient of the liquid.<sup>25,26</sup> Another method is increasing the beam size by moving the liquid away from the focal point of the focusing lens.<sup>15,22,25,27</sup> However, the exact beam size depends on the optics and positioning accuracy, which are difficult to reproduce. Also, the quantitative influence of the beam size on the thermocavitation process and its energy transfer has not been reported yet.

Furthermore, the temperature at the moment of nucleation is still debated. Fluorescent measurements using Rhodamine-B resulted in a maximum temperature of  $98^\circ\text{C}$ .<sup>28</sup> However, the sensitivity of this dye as temperature sensor goes down rapidly above  $80^\circ\text{C}$ ,<sup>29</sup> for which reason any extrapolation to higher temperatures should be carefully

interpreted. Numerical simulations resulted in temperature of 295–332 °C,<sup>22</sup> which is around or even above the spinodal temperature of 305 °C,<sup>30</sup> and therefore unlikely as nucleation at an interface should happen below the spinodal temperature.<sup>31</sup>

In this manuscript, we investigate the influence of the beam size on the thermocavitation process in microfluidic confinement. We compare our experimental results on the bubble nucleation with a numerical heat transfer simulation in COMSOL. These data provide a better understanding of the moment of nucleation and the energy transfer from the CW laser into the bubble. Our results are of relevance for the use of continuous-wave laser-actuated cavitation in needle-free jet injectors as well as other applications of thermocavitation in microfluidic confinement.

Figure 1 shows the experimental setup, consisting of a microfluidic glass chip with two etched channels along the same axis and separated by 30  $\mu\text{m}$ . The right channel ( $L \times W \times H = 2000 \times 100 \times 400 \mu\text{m}^3$ ) is partially filled with Milli-Q water until the variable filling level  $F$ . The left channel is designated for inserting an optical fiber connected to a CW laser. This single-mode optical fiber (Corning SMF-28e) is positioned inside its channel using a motorized three-axis stage (Thorlabs Rollerblock) with micrometer accuracy. This allows for accurate aligning of the fiber tip with respect to the microfluidic channel. Due to the divergence of the laser beam from the fiber tip, the beam radius at the interface of the microfluidic channel can be controlled by the distance  $D$ . Seven beam radii  $B_R$  are used in the experiment between 10 and 36  $\mu\text{m}$ .

The fiber laser (BKtel Photonics, HPFL-2-350-FCAPC) has a variable output power between 0.2 and 2 W at a wavelength of 1950 nm,

which matches the absorption peak of water ( $\alpha \approx 12\,000 \text{ m}^{-1}$ ).<sup>32</sup> The laser has a secondary fiber output at 1% of the nominal power, which is connected to a photodetector (Thorlabs DET05D2) to monitor the output power *in situ* using an oscilloscope (Tektronix MSO2014B).

Upon laser irradiation, the water inside the right channel is heated, and after a short period ( $t_n \sim \text{ms}$ ), nucleation occurs and a fast growing vapor bubble appears. A Photron NOVA SA-X2 high-speed camera was used in combination with a Navitar 12 $\times$  zoom lens and a Schott CV-LS light source for visualization of the bubble dynamics. The camera was used at a frame rate of 225k fps, a resolution of 384  $\times$  96, and a pixel size of 5  $\mu\text{m}$ . Figure 1 (right panel) shows eight typical images during the bubble lifetime. The images were analyzed with a custom-made MATLAB algorithm, which tracks the bubble over time as shown in the red contours. The bubble length is calculated as the area enclosed in the red contour divided by the channel height (400  $\mu\text{m}$ ). The growth velocity is taken by fitting the bubble length of the second to the fifth frame.

The heating phase was simulated in COMSOL until nucleation. First, using the ray optics module, the beam radius in the water channel is obtained for the different fiber positions used in the experiment. These beam radii are then used in the heat transfer module to simulate the heating. The energy absorption is calculated with Lambert–Beer, using the absorption coefficient of water, which reduces with increasing temperature.<sup>33,34</sup> It also includes the loss of heat due to dissipation into the walls of the glass chip. More details regarding the numerical simulations of the ray tracing and heat transfer can be found in the supplementary material Secs. 1 and 2, respectively.

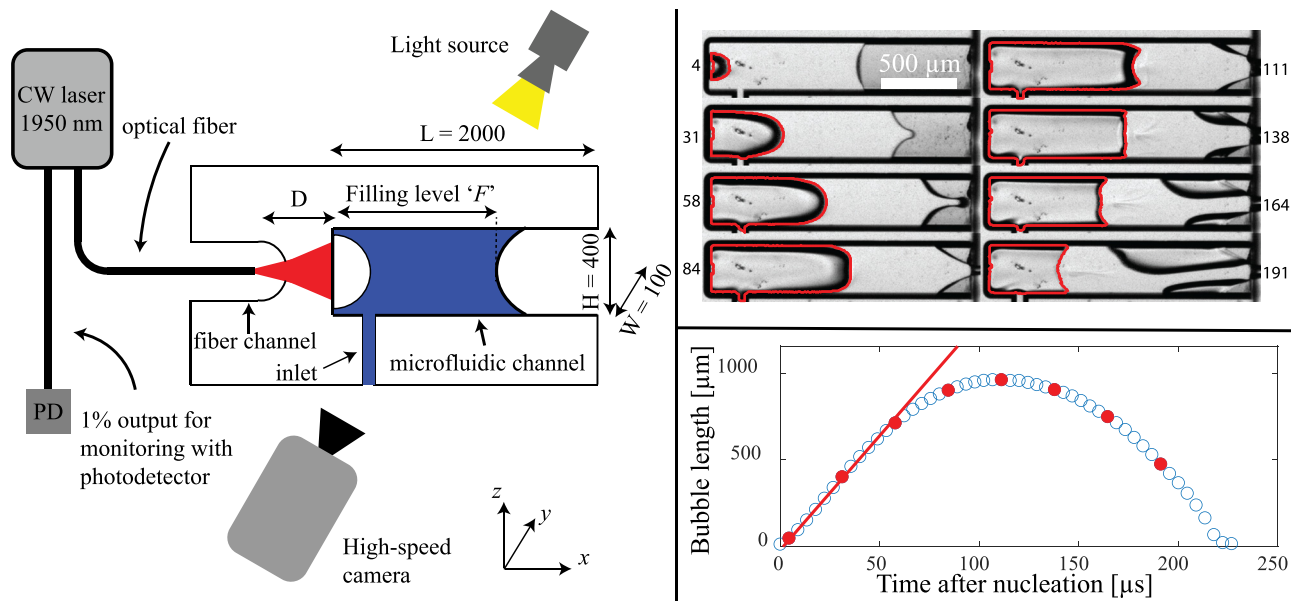


**FIG. 1.** Left: experimental setup consisting of a microfluidic glass chip with two etched channels. The microfluidic channel (right) is filled with water up to distance  $F$ . The output fiber of a CW laser is inserted inside the fiber channel (left) and positioned with micrometer accuracy. The distance between the fiber tip and the microfluidic channel  $D$  defines the beam size of the laser at the glass–liquid interface. Upon laser irradiation, nucleation occurs and a vapor bubble will grow and collapse. A high-speed camera with corresponding light source is positioned along the  $y$  axis. Top right: eight selected experimental images of the bubble and its contour highlighted in red ( $F = 1000 \mu\text{m}$ ,  $P = 550 \text{ mW}$ , and  $B_R = 18.7 \mu\text{m}$ ). The numbers next to the frames indicate the time after nucleation in  $\mu\text{s}$ . Scale bar in the first frame indicates 500  $\mu\text{m}$ . For the full experimental video, see video S1. Bottom right: bubble length plotted vs time after nucleation. Red dots correspond to eight frames above. Growth velocity is fitted from the first five frames, resulting in a slope of 13.2 m/s.

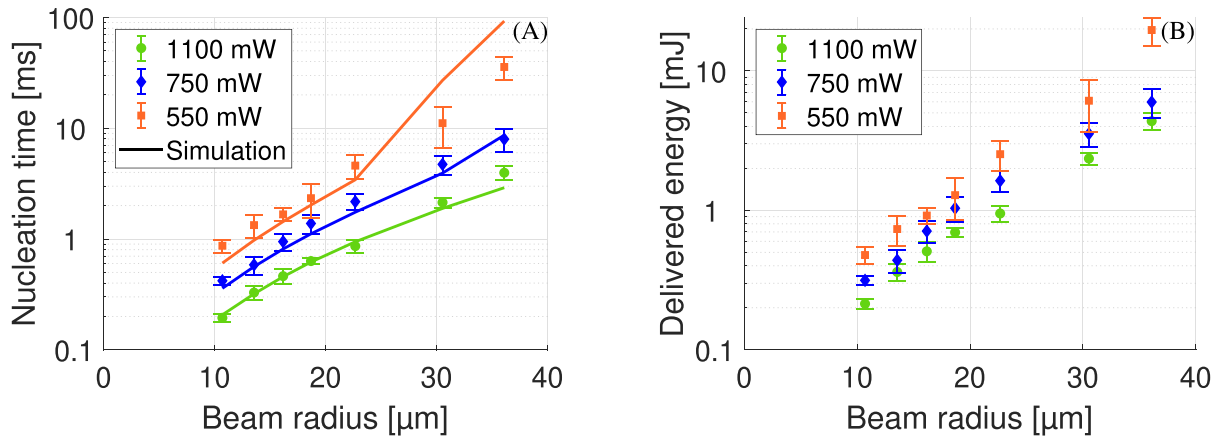


**FIG. 2.** Nucleation time (a) and delivered energy (b) as a function of beam radius, for three different laser powers. The error bars indicate the standard deviation for at least six individual experiments. The solid lines in (a) indicate the time in the COMSOL simulations at which the maximum temperature in the liquid is equal to 237 °C. The delivered energy in (b) is calculated as  $E_d = P_L \times t_n$ .

Figure 2(a) shows the nucleation time as a function of beam radius, for three different laser powers. The data points are averaged over at least six individual measurements, and the error bars indicate the standard deviation. It is clear that the nucleation time increases with increasing beam radius, as well as reducing laser power. These two effects reduce the laser intensity, resulting in slower localized heating of the liquid and therefore a longer nucleation time.

For the middle laser power (750 mW), the experiment was performed for three different filling levels,  $F = 600, 1000,$  and  $1700 \mu\text{m}$ . It was found that the filling level did not have any significant effect on the nucleation time (see Fig. S2 in the supplementary material). This is explained as the filling levels are 8–20 times larger than the absorption length ( $\sim 80 \mu\text{m}$ ), and therefore, the additional liquid has no effect on the heating, as all the optical power is absorbed before the laser beam reaches the meniscus. The typical length over which heat diffusion takes place,  $\delta$ , is calculated as<sup>35</sup>

$$\delta = \sqrt{4\kappa t_n}, \quad (1)$$

where  $\kappa$  is the thermal diffusivity ( $0.14 \text{ mm}^2/\text{s}$  for water). Even for the longest nucleation time (35 ms),  $\delta = 70 \mu\text{m}$ , and therefore at least one order of magnitude smaller than the filling level. Therefore, it can be assumed that changes in the filling level do not affect the nucleation times.

In the numerical simulations using COMSOL, the energy absorption and heat transfer in the liquid experiment is simulated until the moment of nucleation, which we took from the experimental nucleation times. These experimental nucleation times are in agreement with simulated times with a maximum local temperature of 237 °C, see solid lines in Fig. 2(a). This agreement indicates that nucleation temperature is independent of laser beam radius and power. However, the two lowest laser intensities show an exception, where the beam radius is large and laser power small. In such cases, the experiment gives a smaller temperature due to a larger heated region, which is up to 30 times larger compared to the other cases. In such situations, nucleation may happen at lower temperatures, and thus shorter nucleation times. For all other data points, the temperature is very close to the 237 °C, with a standard deviation of 5 °C (see Fig. S3 in the

supplementary material). These temperatures are well above the boiling temperature of water (100 °C), which is explained by the existence of an energy barrier for nucleation. Due to this energy barrier, higher temperatures are needed for bubble formation in microfluidic volumes on short timescales (ms). On the other hand, these temperatures are well below the spinodal temperature at atmospheric pressure (306 °C),<sup>30</sup> which is explained as the bubble forms at a wall, where the energy barrier for bubble formation is lower.<sup>36</sup> Due to this energy barrier, the nucleation itself is a stochastic event,<sup>22,30</sup> which could further explain the slight variations in nucleation time and temperature.

In the literature, different temperatures are noted for bubble formation using a CW laser, either through thermocavitation<sup>22,28</sup> (direct heating of the liquid) or plasmonic heating<sup>23,37,38</sup> (indirect heating of the liquid through plasmonic nanoparticles), see Fig. 3. For thermocavitation, studies report different values, either close to the boiling temperature or the spinodal temperature, both of which are unlikely due to the above-mentioned reasons. Our values are in agreement with temperatures found for plasmonic bubbles; therefore, we conclude that our values are closer to the actual temperatures in thermocavitation. Nonetheless, heterogeneous nucleation depends on impurities, which

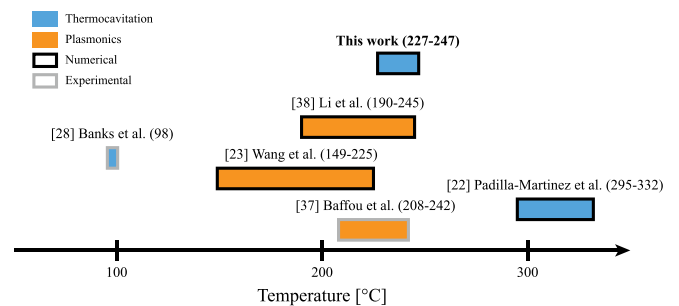


**FIG. 3.** Calculated temperature ranges for nucleation in water with continuous-wave lasers found in the literature. Blue colors indicate thermocavitation and orange plasmonic heating. Black outlines indicate numerical calculations, and gray outline indicates experimental measurements. They appear in chronological order, with earliest work at the bottom.

act as nucleation sites.<sup>30,39</sup> These impurities, such as surface roughness,<sup>36</sup> surfactants, or dissolved gas molecules,<sup>40,41</sup> reduce the energy barrier and therefore result in earlier nucleation.

Figure 2(b) shows the delivered energy at the moment of nucleation as a function of beam radius, which is calculated by the laser power multiplied by the nucleation time ( $E_d = P_L \times t_n$ ). We observe an increase in beam radius or decrease in laser power results in an increase in energy. Furthermore,  $E_d$  spans over two orders of magnitude (0.2–20 mJ), for a single thermocavitation setup. Especially, the beam radius plays a significant role in the delivered energy, which makes this setup an optimal way to accurately control the amount of delivered energy.

The maximum bubble volumes are shown in Fig. 4(a) as a function of delivered energy. For all experimental parameters, the maximum bubble volume increases linearly with delivered energy (see logarithmic slope of 1). As all data points are along the same curve, there is little influence of laser power or filling level. However, for large values of delivered energies ( $E_d \geq 2$  mJ), the bubble volume plateaus. This plateau is explained by the limited channel length, as the bubble collapses at the moment they coalesce with the surrounding air (see example in Fig. S4 and Video S2 in the supplementary material). Therefore, the bubble never reaches its potential maximum volume, and larger bubbles cannot be observed in this configuration. This is most apparent for the smallest filling level (black squares), where already for smaller bubble volumes it can coalesce with the air inside the channel, resulting in lower plateau values in Fig. 4(a).

Figure 4(b) shows the kinetic energy of the bubble as a function of delivered energy. The kinetic energy is  $E_{kin} = \frac{1}{2}mv^2$ , where  $m$  is the liquid mass in the channel, and  $v$  the maximum bubble growth velocity (change of length over per unit time). We note that the bubble kinetic energy increases quadratically (log slope = 2) with the delivered energy, independent of the laser or liquid parameters. This means that for a constant filling level, the bubble growth rate increases linearly with the delivered energy, as was also found in our earlier work.<sup>21</sup> Here, we now also find that the mass ( $m \propto F$ ) does not affect the energy transfer, and therefore, the bubble growth rate  $v$  scales with  $v \propto F^{-0.5}$ , which matches previous qualitative observations.<sup>42</sup> For applications, such as jet formation for printing or needle-free injection, this

means that the liquid velocity can be controlled through the mass of liquid in the confinement or the beam radius (see Fig. S5 in the supplementary material). This dependence of laser parameters contrasts with pulsed lasers, where an increase in the beam radius results in a slower growing bubble.<sup>19,21</sup> For large values of the delivered energy, the slope in Fig. 4(b) decreases. This is explained by heat diffusion, as this large amount of energy is achieved through long nucleation times, at which point heat dissipation into the glass plays a significant role [see Eq. (1)]. This is especially the case for the smallest laser power (pink stars), which requires the longest nucleation times to reach those energies, resulting in more heat dissipation.

One of the goals of the COMSOL simulations was to investigate the heat dissipation during the absorption of optical energy until moment of nucleation. As discussed in the previous subsection, nucleation happens at approximately 237 °C. However, after nucleation has occurred and the energy barrier has been overcome, liquid at a lower temperature (but still above 100 °C) may also contribute to this growing bubble. Figure 5 shows the bubble kinetic energy as a function of the volume of superheated water ( $T > 100$  °C) at the moment of nucleation. This superheated volume is taken from the COMSOL simulations at the moment of nucleation in the experiment. In contrast to Fig. 4(b), where the initial quadratic relation seems to decrease, the slope in Fig. 5 remains constant, which is explained as heat dissipation is included in this simulation.

Microbubbles can also be created by different means, such as pulsed lasers,<sup>21</sup> plasmonic bubbles,<sup>38</sup> voltage discharge,<sup>43,44</sup> microheaters,<sup>45</sup> and the tube arrest method.<sup>46</sup> These methods can create similar bubble sizes as in this study and require similar amounts of energy.<sup>21,43</sup> Follow-up studies could focus on a quantitative comparison between the bubble dynamics to find the best method for different applications. However, most of these methods are invasive, which reduces the ease of use and making chip fabrication more complex. The laser-generated bubbles allow for local heating and generation of bubbles on-chip, and more specifically the use of CW lasers allow for small and affordable setup.

We proposed and developed a setup to accurately control the laser beam size for thermocavitation in microfluidic confinement. We compared experimental results using high-speed imaging to numerical

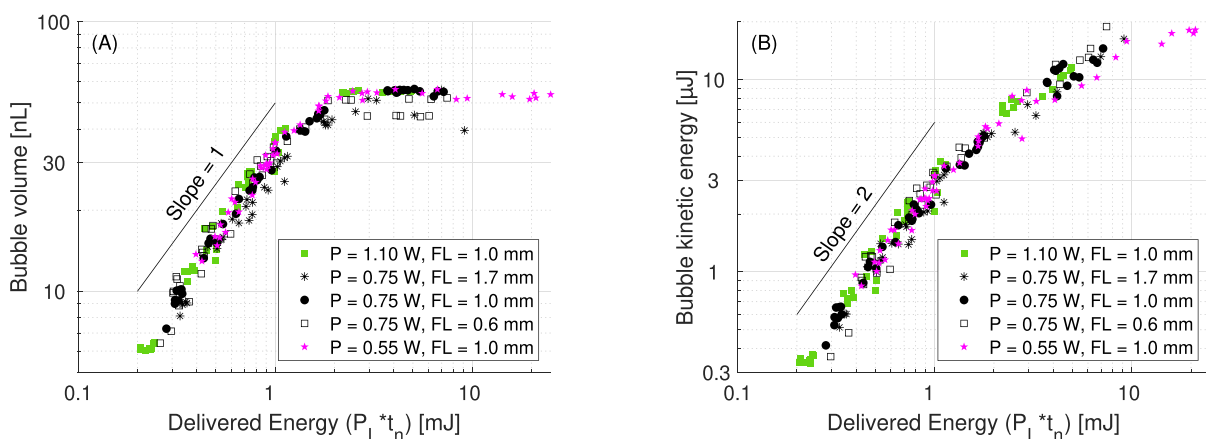
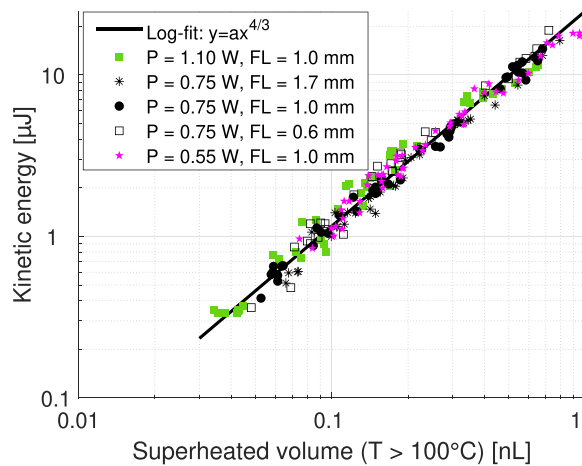


FIG. 4. Bubble volume (a) and kinetic energy (b) vs delivered energy, for different laser powers  $P$  and filling levels  $F$ . Volume is calculated from bubble area multiplied by the channel depth (100  $\mu\text{m}$ ). Kinetic energy  $E_{kin} = \frac{1}{2}mv^2$ , where  $m$  is the liquid mass in the channel, and  $v$  the maximum bubble growth velocity.



**FIG. 5.** Bubble kinetic energy vs volume of superheated liquid ( $T > 100^\circ\text{C}$ ) at the moment of nucleation, taken from the simulation. Each data point is an individual experiment, where the color and symbol indicate the laser power and filling level. Solid black line is logarithmic fit with slope of  $4/3$ , where  $a = 25 \mu\text{J}/\text{nL}^{4/3}$ .

simulations on the energy absorption and heat transfer. This study focused on the influence of laser beam characteristics on thermocavitation in microfluidic confinement and the energy conversion. We found that the nucleation time increases with increasing beam radius as well as decreasing laser power. Numerical simulations of the heat transfer show that the maximum temperature at the moment of nucleation is  $237 \pm 10^\circ\text{C}$  and independent of laser beam parameters. This temperature is below the spinodal temperature ( $306^\circ\text{C}$ ), but well above the boiling temperature ( $100^\circ\text{C}$ ) and is in agreement with earlier work on plasmonic bubbles. As the filling level  $F$  is much larger than the absorption length, it does not influence the nucleation time or temperature, but only the bubble dynamics after nucleation, due to the increased mass of liquid.

Furthermore, we found that the maximum bubble volume increases linearly with delivered energy and the conversion is independent of laser parameters. For the largest energies, the maximum bubble volume reaches a plateau as the bubble coalesces with the surrounding air before it reaches its maximum potential volume. The bubble kinetic energy increases quadratically with the delivered energy. However, for large energies, heat dissipation decreases the conversion efficiency, as the nucleation time is on the same timescale as thermal diffusion. From the temperature profiles in the numerical simulations, we find that the bubble kinetic energy increases with volume of superheated liquid ( $T > 100^\circ\text{C}$ ), with a power law of  $4/3$ . As heat dissipation is included in these simulations, this relation holds for all data points, independent of the laser or liquid parameters.

Our findings contribute to the understanding and use of thermocavitation and allow for a better control over the bubble characteristics in real life applications. The laser power and beam radius control the nucleation time and delivered energy and can therefore control the bubble size and growth rate. This allows for optimal use of thermocavitation in a wide range of applications, including laser-actuated jet injection.

See the supplementary material for more information regarding the simulations, as well as additional figures of the nucleation temperatures and bubble dynamics. Video S1 corresponds to the bubble shown in Fig. 1, and Video S2 corresponds to the bubble shown in Fig. S4.

J.J.S and D.F.R. acknowledge the funding from the European Research Council (ERC) under the European Union's Horizon 2020 Research and Innovation Programme (Grant Agreement No. 851630). J.J.S. would like to thank Stefan Schlautmann for the fabrication of the microfluidic chips and Nicolás Rivera Bueno for his work on preliminary numerical simulations.

## AUTHOR DECLARATIONS

### Conflict of Interest

David Fernandez Rivas is co-founder of FlowBeams, a spin-off company of the University of Twente on laser-actuated needle-free injection.

### Author Contributions

**Jelle J. Schoppink:** Conceptualization (lead); Data curation (lead); Formal analysis (lead); Investigation (lead); Methodology (lead); Visualization (lead); Writing – original draft (lead). **Jose A. Alvarez-Chavez:** Conceptualization (equal); Writing – review & editing (equal). **David Fernandez Rivas:** Conceptualization (equal); Funding acquisition (equal); Project administration (equal); Supervision (equal); Writing – review & editing (equal).

## DATA AVAILABILITY

The data that support the findings of this study are available from the corresponding author upon reasonable request.

## REFERENCES

- <sup>1</sup>S. F. Rastopov and A. T. Sukhodol'skii, "Self-organization of the heat cycle due to thermal cavitation during continuous laser heating of a liquid," *Sov. Phys. Dokl.* **32**, 671 (1987).
- <sup>2</sup>V. M. Chudnovskii, V. I. Yusupov, A. V. Dydykin, V. I. Nevozhai, A. Y. Kisilev, S. A. Zhukov, and V. N. Bagratashvili, "Laser-induced boiling of biological liquids in medical technologies," *Quantum Electron.* **47**, 361–370 (2017).
- <sup>3</sup>S. M. Afanador-Delgado, V. F. Marañón-Ruiz, R. Sevilla-Escoboza, and R. Chiu, "Synthesis of  $\text{SiO}_2$  nanoparticles assisted by thermocavitation in natural dye (*Hibiscus sabdariffa* L.)," *Opt. Laser Technol.* **147**, 107559 (2022).
- <sup>4</sup>V. Korede, N. Nagalingam, F. Marques, N. van der Linden, J. T. Padding, R. Hartkamp, and H. B. Eral, "A review on laser-induced crystallization from solution," *Cryst. Growth Des.* **23**, 3873–3916 (2023).
- <sup>5</sup>N. G. García-Morales, B. Morales-Cruzado, S. Camacho-López, R. Romero-Méndez, L. F. Devia-Cruz, and F. G. Pérez-Gutiérrez, "Numerical modeling of a micropump without mobile parts actuated by thermocavitation bubbles," *Microsyst. Technol.* **27**, 801–812 (2021).
- <sup>6</sup>R. Zaca Moran, C. Amaxal-Cuatel, P. Zaca-Moran, J. Castillo Mixcoatl, R. Ramos-García, and J. P. Padilla-Martínez, "Thermocavitation: A novel mechanism to pulse fiber lasers," *Opt. Express* **29**, 23439–23446 (2021).
- <sup>7</sup>A. Guzmán-Barraza, J. Ortega-Mendoza, P. Zaca-Morán, N. Toto-Arellano, C. Toxqui-Quitl, and J. Padilla-Martínez, "Optical cavitation in non-absorbent solutions using a continuous-wave laser via optical fiber," *Opt. Laser Technol.* **154**, 108330 (2022).
- <sup>8</sup>N. Korneev, P. R. Montero, R. Ramos-García, J. C. Ramírez-San-Juan, and J. P. Padilla-Martínez, "Ultrasound induced by CW laser cavitation bubbles," *J. Phys.: Conf. Ser.* **278**, 012029 (2011).

- <sup>9</sup>R. Zaca Moran, J. Castillo Mixcoatl, N. E. Sierra-Gonzalez, J. M. Perez Corte, P. Zaca-Moran, J. Ramirez-San-Juan, R. Ramos-Garcia, and J. P. Martinez, "Theoretical and experimental study of acoustic waves generated by thermocavitation and its application in the generation of liquid jets," *Opt. Express* **28**, 4928–4937 (2020).
- <sup>10</sup>J. A. Sarabia-Alonso, J. G. Ortega-Mendoza, J. C. Ramirez-San-Juan, P. Zaca-Morán, J. Ramirez-Ramírez, A. Padilla-Vivanco, F. M. Muñoz-Pérez, and R. Ramos-Garcia, "Optothermal generation, trapping, and manipulation of microbubbles," *Opt. Express* **28**, 17672 (2020).
- <sup>11</sup>J. A. Sarabia-Alonso, J. G. Ortega-Mendoza, S. Mansurova, F. M. Muñoz-Pérez, and R. Ramos-Garcia, "3D trapping of microbubbles by the Marangoni force," *Opt. Lett.* **46**, 5786 (2021).
- <sup>12</sup>J. Schoppink and D. Fernandez Rivas, "Jet injectors: Perspectives for small volume delivery with lasers," *Adv. Drug Delivery Rev.* **182**, 114109 (2022).
- <sup>13</sup>D. L. van der Ven, D. Morrone, M. A. Quetzeri-Santiago, and D. F. Rivas, "Microfluidic jet impact: Spreading, splashing, soft substrate deformation and injection," *J. Colloid Interface Sci.* **636**, 549–558 (2023).
- <sup>14</sup>J. J. Schoppink, K. Mohan, M. A. Quetzeri-Santiago, G. McKinley, D. F. Rivas, and A. K. Dickerson, "Cavitation-induced microjets tuned by channels with alternating wettability patterns," *Phys. Fluids* **35**, 032017 (2023).
- <sup>15</sup>N. E. González-sierra, J. M. Perez-corte, J. P. Padilla-martinez, S. Cruz-vanegas, and S. Bonfadini, "Bubble dynamics and speed of jets for needle-free injections produced by thermocavitation," *J. Biomed. Opt.* **28**, 1–19 (2023).
- <sup>16</sup>T.-h. Han and J. J. Yoh, "A laser based reusable microjet injector for transdermal drug delivery," *J. Appl. Phys.* **107**, 103110 (2010).
- <sup>17</sup>Y. Tagawa, N. Oudalov, A. E. Ghalbzouri, C. Sun, and D. Lohse, "Needle-free injection into skin and soft matter with highly focused microjets," *Lab Chip* **13**, 1357 (2013).
- <sup>18</sup>J. Krizek, P. Delrot, and C. Moser, "Repetitive regime of highly focused liquid microjets for needle-free injection," *Sci. Rep.* **10**, 5067 (2020).
- <sup>19</sup>J. Krizek, F. D. Goumoëns, P. Delrot, and C. Moser, "Needle-free delivery of fluids from compact laser-based jet injector," *Lab Chip* **20**, 3784 (2020).
- <sup>20</sup>M. Moradifrapoli and J. O. Marston, "High-speed video investigation of jet dynamics from narrow orifices for needle-free injection," *Chem. Eng. Res. Des.* **117**, 110 (2017).
- <sup>21</sup>J. J. Schoppink, J. Krizek, C. Moser, and D. Fernandez Rivas, "Cavitation induced by pulsed and continuous-wave fiber lasers in confinement," *Exp. Therm. Fluid Sci.* **146**, 110926 (2023).
- <sup>22</sup>J. P. Padilla-Martinez, C. Berrospe-Rodriguez, G. Aguilar, J. C. Ramirez-San-Juan, and R. Ramos-Garcia, "Optic cavitation with CW lasers: A review," *Phys. Fluids* **26**, 122007 (2014).
- <sup>23</sup>Y. Wang, M. E. Zaytsev, G. Lajoinie, H. L. The, J. C. Eijkel, A. van den Berg, M. Versluis, B. M. Weckhuysen, X. Zhang, H. J. Zandvliet, and D. Lohse, "Giant and explosive plasmonic bubbles by delayed nucleation," *Proc. Natl. Acad. Sci. U. S. A.* **115**, 7676 (2018).
- <sup>24</sup>J. Ramirez-San-Juan, E. Rodriguez-Aboytes, A. E. Martinez-Canton, O. Baldovino-Pantaleon, A. Robledo-Martinez, N. Korneev, and R. Ramos-Garcia, "Time-resolved analysis of cavitation induced by CW lasers in absorbing liquids," *Opt. Express* **18**, 8735 (2010).
- <sup>25</sup>B. Zhang, D. Banks, V. Robles, L. Felipe, D. Cruz, and G. Aguilar, "High resolution optical investigation of laser intensity and solution temperature effects on thermocavitation," *Exp. Therm. Fluid Sci.* **136**, 110683 (2022).
- <sup>26</sup>S. M. Afanador-Delgado, R. Sevilla-Escoboza, V. F. Marañón-Ruiz, and R. Chiu, "Influence of the anthocyanin concentration in ethanolic extracts of *Hibiscus Sabdariffa* on thermocavitation: An analysis of the pulse frequency and amplitude," *Opt. Laser Technol.* **132**, 106468 (2020).
- <sup>27</sup>J. P. Padilla-Martinez, G. Aguilar, J. C. Ramirez-San-Juan, and R. Ramos-Garcia, "Temporal evolution of thermocavitation bubbles using high speed video camera," *Proc. SPIE* **8097**, 809727 (2011).
- <sup>28</sup>D. Banks, V. Robles, B. Zhang, L. F. Devia-Cruz, S. Camacho-Lopez, and G. Aguilar, "Planar laser induced fluorescence for temperature measurement of optical thermocavitation," *Exp. Therm. Fluid Sci.* **103**, 385–393 (2019).
- <sup>29</sup>D. Ross, M. Gaitan, and L. E. Locascio, "Temperature measurement in microfluidic systems using a temperature-dependent fluorescent dye," *Anal. Chem.* **73**, 4117–4123 (2001).
- <sup>30</sup>F. Caupin and E. Herbert, "Cavitation in water: A review," *C. R. Phys.* **7**, 1000–1017 (2006).
- <sup>31</sup>C. T. Avedisian, "The homogeneous nucleation limits of liquids," *J. Phys. Chem. Ref. Data* **14**, 695–729 (1985).
- <sup>32</sup>R. Deng, Y. He, Y. Qin, Q. Chen, and L. Chen, "Measuring pure water absorption coefficient in the near-infrared spectrum (900–2500 nm)," *J. Remote Sens.* **16**, 192–206 (2012).
- <sup>33</sup>E. D. Jansen, T. G. van Leeuwen, M. Motamedi, C. Borst, and A. J. Welch, "Temperature dependence of the absorption coefficient of water for mid-infrared laser radiation," *Lasers Surg. Med.* **14**, 258–268 (1994).
- <sup>34</sup>B. I. Lange, T. Brendel, and G. Hüttmann, "Temperature dependence of light absorption in water at holmium and thulium laser wavelengths," *Appl. Opt.* **41**, 5797 (2002).
- <sup>35</sup>G. Paltauf and P. E. Dyer, "Photomechanical processes and effects in ablation," *Chem. Rev.* **103**, 487–518 (2003).
- <sup>36</sup>A. A. Atchley and A. Prosperetti, "The crevice model of bubble nucleation," *J. Acoust. Soc. Am.* **86**, 1065–1084 (1989).
- <sup>37</sup>G. Baffou, J. Polleux, H. Rigneault, and S. Monneret, "Super-heating and micro-bubble generation around plasmonic nanoparticles under cw illumination," *J. Phys. Chem. C* **118**, 4890–4898 (2014).
- <sup>38</sup>X. Li, Y. Wang, M. E. Zaytsev, G. Lajoinie, H. Le The, J. G. Bomer, J. C. Eijkel, H. J. Zandvliet, X. Zhang, and D. Lohse, "Plasmonic bubble nucleation and growth in water: Effect of dissolved air," *J. Phys. Chem. C* **123**, 23586 (2019).
- <sup>39</sup>A. Prosperetti, "Vapor bubbles," *Annu. Rev. Fluid Mech.* **49**, 221 (2017).
- <sup>40</sup>M. S. Pettersen, S. Balibar, and H. J. Maris, "Experimental investigation of cavitation in superfluid <sup>4</sup>He," *Phys. Rev. B* **49**, 12062–12070 (1994).
- <sup>41</sup>P. Pfeiffer, J. Eisener, H. Reese, M. Li, X. Ma, C. Sun, and C.-D. Ohl, "Thermally assisted heterogeneous cavitation through gas supersaturation," *Phys. Rev. Lett.* **128**, 194501 (2022).
- <sup>42</sup>L. Oyarte Gálvez, A. Fraters, H. L. Offerhaus, M. Versluis, I. W. Hunter, and D. Fernández Rivas, "Microfluidics control the ballistic energy of thermocavitation liquid jets for needle-free injections," *J. Appl. Phys.* **127**, 104901 (2020).
- <sup>43</sup>D. Podbevšek, Ž. Lokar, J. Podobnikar, R. Petkovšek, and M. Dular, "Experimental evaluation of methodologies for single transient cavitation bubble generation in liquids," *Exp. Fluids* **62**, 167 (2021).
- <sup>44</sup>S. R. Gonzalez Avila, C. Song, and C.-D. Ohl, "Fast transient microjets induced by hemispherical cavitation bubbles," *J. Fluid Mech.* **767**, 31 (2015).
- <sup>45</sup>D. M. Nguyen, M. S. Sanathanan, J. Miao, D. F. Rivas, and C. D. Ohl, "In-phase synchronization between two auto-oscillating bubbles," *Phys. Rev. Fluids* **4**, 43601 (2019).
- <sup>46</sup>H. Bao, F. Reuter, H. Zhang, J. Lu, and C. D. Ohl, "Impact-driven cavitation bubble dynamics," *Exp. Fluids* **64**, 1–13 (2023).